Marine Pollution Bulletin 217 (2025) 118137

Contents lists available at ScienceDirect

Marine Pollution Bulletin

journal homepage: www.elsevier.com/locate/marpolbul

Microbial pterin biomolecules facilitate algal blooms in response to nutrient pressure in estuarine and coastal continuum

Kang Mei [a,b,h,*], Yitong Pan [c], Faisal Hamzah [b,d], Mohammad Mazbah Uddin [e], Xuri Dong [a], Lizhe Cai [f], Bin Xie [g,**], Nengwang Chen [b,f], Deli Wang [b,h,**]

[a] Jiangsu Institute of Marine Resources Development, Jiangsu Key Laboratory of Marine Bioresources and Environment, Jiangsu Ocean University, Lianyungang 222005, China
[b] State Key Laboratory of Marine Environmental Science, College of Ocean and Earth Sciences, Xiamen University, Xiamen 361102, China
[c] Department of Civil and Environmental Engineering, Princeton University, Princeton, NJ 08544, USA
[d] Research Center for Oceanography, National Research and Innovation Agency, Jakarta 10340, Indonesia
[e] Key Laboratory of the Ministry of Education for Earth Surface Processes & College of Urban and Environmental Sciences, Peking University, Beijing 100089, China
[f] Key Laboratory of Ministry of Education for Coastal and Wetland Ecosystems, College of the Environment and Ecology, Xiamen University, Xiamen 361102, China
[g] Key Laboratory of Marine Ecological Conservation and Restoration, Third Institute of Oceanography, Ministry of Natural Resources, Xiamen 361005, China
[h] Jiangsu Marine Resources Development Technology Innovation Center, Lianyungang 222042, China

ARTICLE INFO

Keywords:
Microbial pterins
Spatiotemporal variation
Phytoplankton
Excessive nutrients
Bioindicator

ABSTRACT

Pterins are ubiquitous biomolecules synthesized by diverse phytoplankton, serve as pigments, cofactors, precursors, and redox sensors, playing crucial roles in ocean carbon fixation and nutrient cycling. However, the mechanisms driving their production, distribution, and fate in marine ecosystems are not well understood. This study examines the generation and behavior of microbial pterins in the Jiulong River Estuary, a system affected by nutrient-rich discharges. Results reveal distinct patterns: pterin concentrations remain uniform across water columns during flood periods but vary significantly during dry periods. During flooding, microbial pterins rank as isoxanthopterin > neopterin > dihydroneopterin > biopterin, while biopterin and isoxanthopterin dominate during dry conditions. Elevated pterin levels in the upper estuary during flooding suggest rapid production in response to nutrient influx, which drives algal proliferation. Positive correlations between pterins and chlorophyll-a (chl-a) highlight photoautotrophic microbes as primary contributors. Notably, cellular biopterin peaks during exponential algal growth, indicating its preparatory role in bloom proliferation. As dual biomarkers with chl-a, microbial pterins enhance the specificity of bloom detection and offer insights into bloom dynamics and nutrient-driven changes. These findings underscore the ecological significance of pterins in nutrient cycling and their potential as bioindicators, warranting further research into their broader environmental implications.

1. Introduction

Pterins represent a class of biologically essential heterocyclic compounds that serve fundamental roles across multiple biochemical systems. These ubiquitous biomolecules, synthesized by diverse microorganisms, participate critically in various biosynthetic pathways (Basu and Burgmayer, 2011; Feirer and Fuqua, 2017). The prebiotic synthesis of pterins under laboratory conditions underscores their significance in the evolution from abiotic to biotic processes (Enchev and Slavova, 2021; Marín-Yaseli et al., 2015; Menor-Salván et al., 2022; Rodriguez et al., 2024). Particularly noteworthy is the hypothesized role of formyl pterins at alkaline vent-ocean interfaces, where they may serve as crucial intermediates in the Wood-Ljungdahl pathway and purine biosynthesis (Martin and Russell, 2007).

In contemporary biological systems, pterins demonstrate remarkable functional diversity. They serve as both pigments and enzymatic cofactors in bacterial systems, forming essential precursors for key biomolecules including folic acid (B9), riboflavin (B2), and cobalamin (B12) (Suffridge et al., 2017; Taira and Nawa, 1958). The biosynthesis of pterins initiates with GTP cyclohydrolase converting GTP into dihydro-

* Correspondence to: K. Mei, Jiangsu Institute of Marine Resources Development, Jiangsu Key Laboratory of Marine Bioresources and Environment, Jiangsu Ocean University, Lianyungang 222005, China.
** Corresponding authors.
E-mail addresses: kangmei@jou.edu.cn (K. Mei), xiebin@tio.org.cn (B. Xie), deliwang@xmu.edu.cn (D. Wang).

https://doi.org/10.1016/j.marpolbul.2025.118137
Received 9 February 2025; Received in revised form 25 April 2025; Accepted 8 May 2025
Available online 11 May 2025

neopterin triphosphate, a central precursor for various pterin derivatives including folate, neopterin, monapterin, and biopterin (Feirer and Fuqua, 2017). Pterins exhibit redox-dependent photochemical duality: in their reduced forms, they serve as antioxidants that mitigate oxidative stress, whereas oxidized aromatic pterins (including biopterin and neopterin) function as endogenous Type I photosensitizers capable of mediating phototoxic damage to biomolecules through radical generation pathways (Lorente et al., 2021). As efficient singlet oxygen photosensitizers, pterin derivatives demonstrate significant quantum yields of singlet oxygen production while also exhibiting notable quenching capabilities (Oliveros et al., 2010; Thomas et al., 2003). Pterin derivatives can induce oxidative damage to nucleic acids under UV-A exposure, with pterin and its C6-substituted derivatives (6-carboxypterin and 6-formylpterin) being particularly efficient photosensitizers through electron transfer mechanisms (Petroselli et al., 2008; Serrano et al., 2017, 2015, 2012). This dual functionality - encompassing both protective and potentially damaging roles - underscores the complex nature of pterins in biological and photochemical systems (Dantola et al., 2017).

The structural diversity of pterins is further exemplified by their frequent conjugation with glycosides and nucleotides (Basu and Burgmayer, 2011; Buglak et al., 2022; Feirer and Fuqua, 2017; Mahendran et al., 2020). Cyanobacterial pterins have been associated with phenotypes or light signal transduction related to UV protection and phototaxis (Moon et al., 2010a, 2010b; Wachi et al., 1995). Structurally, pterins are often conjugated with glycosides and nucleotides (Buglak et al., 2022; Feirer and Fuqua, 2017; Noguchi et al., 1999; Saito et al., 2003; Wachi et al., 1995), exemplified by biopterin glucosides, which were initially confirmed in cyanobacteria such as *Anacystis*, *Anabaena*, and *Nostoc* (Forrest et al., 1958; Hatfield et al., 1961). Biopterin glucosides serve crucial photoprotective functions. These compounds absorb UV-A radiation, enhance photosynthetic efficiency (Matsunaga et al., 1993; Wachi et al., 1995), and prevent UV-induced degradation of photosynthetic pigments including chlorophyll-a, phycocyanin, and carotenoids in organisms like *Spirulina platensis* (Noguchi et al., 1999; Wachi et al., 1995). Recent studies have further associated pterins with algal-derived organic matter, suggesting their potential as biomarkers for cyanobacterial activity (Yanting Zuo et al., 2021). However, significant gaps remain in our understanding of pterin generation mechanisms, distribution patterns, and ecological roles in marine environments.

Estuarine ecosystems, occupying the critical interface between terrestrial and marine environments, face increasing anthropogenic pressures that significantly alter their biogeochemical processes (Cai et al., 2021; Mao et al., 2022; Wang and Wang, 2016). These systems exhibit substantial variability in hydrochemical parameters (temperature, salinity, pH, dissolved oxygen) due to complex interactions between hydrological and biogeochemical factors (Wang et al., 2011, 2012). These variations are influenced by factors including organic and inorganic complexation (Batchelli et al., 2010; Bruland and Lohan, 2006), adsorption-desorption dynamics of particles (Powell et al., 1996; Roy et al., 2011), as well as particulate co-precipitation and re-release mechanisms (Fang and Wang, 2022; Pokrovsky et al., 2014). Additionally, the unregulated, high-density expansion of nearshore marine aquaculture in southeast China has resulted in pollution, habitat degradation, and sea-use conflicts. Human-induced environmental pollution, particularly eutrophic nutrients, and heavy metals, has disrupted coastal macrozoobenthic communities (Mei et al., 2024; Uddin et al., 2024; Zhao et al., 2024). Land-derived nutrients undergo complex transformations before entering marine systems (Jing, 1995; Mei et al., 2024; Wang et al., 2012), frequently triggering algal blooms that favor cyanobacterial dominance. This influx accelerates eutrophication and the frequency of algal blooms, which severely threaten ecological health by promoting the overgrowth of phytoplankton, including algae and cyanobacteria (Zhang et al., 2023). Recent research on nutrient and salt pollution in stream microcosms revealed a rapid shift from diatoms and green algae to cyanobacteria, accompanied by rising chl-a levels within 14 days (Salcedo et al., 2024).

The primary objective of this study was to evaluate microbial pterins as potential bioindicators, offering novel insights into estuarine ecological processes. To the best of our knowledge, very few studies have focused on nutrient supply and microbial pterin accumulation concerning phytoplankton growth across the estuarine and coastal continuum. In this study, we analyzed dissolved inorganic nitrogen species (NO_3^-, NO_2^-, and NH_4^+), phosphate, microbial pterins, chl-a, and microbial composition in the surface and bottom waters, alongside key biogeochemical parameters at the Jiulong River Estuary. This study was designed to specifically address the following objectives: (i) to elucidate the generation, occurrence, behavior, and fate of microbial pterins in the estuarine and coastal continuum. Specifically, we identified and quantified microbial biopterin (Bip), neopterin (Nep), 7,8-dihydroneopterin (H2Dep), and isoxanthopterin (Ixp), derived from GTP metabolism, which has been linked to phytoplankton growth and bacteria proliferation in previous studies (Lee et al., 1999; McNutt Jr, 1963; Noguchi et al., 1999; Saito et al., 2003; Wachi et al., 1995; Yanting Zuo et al., 2021). (ii) We cultured phytoplankton under dissolved inorganic nitrogen-enriched conditions to examine pterin production in microalgae and the biomass response of the cyanobacterium *Synechococcus* to nutrient pressure. (iii) By investigating the spatiotemporal distribution and biogeochemical dynamics of ubiquitous microbial pterins, this work aims to highlight their role in microorganism-environment interactions and extreme algal blooms under estuarine eutrophic stress. We propose that systematic observations integrating natural and anthropogenic impacts can enhance coastal environmental management strategies.

2. Materials and methods

2.1. Study area

Jiulong River is the second-largest river in Fujian Province, stretching 258 km with a drainage area of 15,000 km^2 (Wang et al., 2017), located in subtropical southeastern China (24°24′–24°36′N, 117°40′–118°16′E, Fig. 1). The Jiulong River Estuary (JRE) spans 100 km^2, connecting Xiamen Bay (XMB, 24° 30′ N, 118° 50′ E) and Taiwan Strait, with water depths range from 3 to 18 m (Yu et al., 2019). The JRE flows into Xiamen Bay primarily through the southeast channel (Guo, 2005). The XMB is situated at the Taiwan Strait's southwest entrance and connected with the South China Sea and the Pacific Ocean (Chen et al., 2021). The semi-enclosed JRE experiences regular semi-diurnal tides and a subtropical monsoon climate, with a wet season from May to September and a dry season from October to April (Han, 2019; Pan et al., 2021). The average monthly rainfall is 4.07 mm day^{-1}. The surface water temperature ranges from 13 to 25 °C, and salinity ranges from 0 to 33 PSU (Ma and Han, 2024).

2.2. Field sampling and processing

Samples were collected from the JRE and the coastal area in the XMB as shown in Fig. 1. The study area of the sampled estuary-nearshore waters was divided into the following according to the geographical distribution: ① the JRE includes the agricultural river section (A3-A10) and the adjacent stations of Jiyu (JY1-JY3), and ② the stations of XMB (X1-X13). Surface and bottom water samples were collected in the summer (July 2021) and autumn (November 2021) by using a GO-FLO water collector (General Oceanics, USA). The samples were stored in high-density polyethylene (HDPE) bottles and pre-filtered on board using a 10-μm nylon sieve to remove impurities. Subsequently, a polycarbonate membrane (47 mm, 0.2 μm, Millipore Germany) filtration was employed at a low pumping pressure (<150 mmHg) to separate particulate samples (0.2–10 μm) from 1 L pre-filtered seawater sample for microbial composition analysis. Particulate samples from 0.5 L pre-filtered seawater were collected under clean conditions to determine

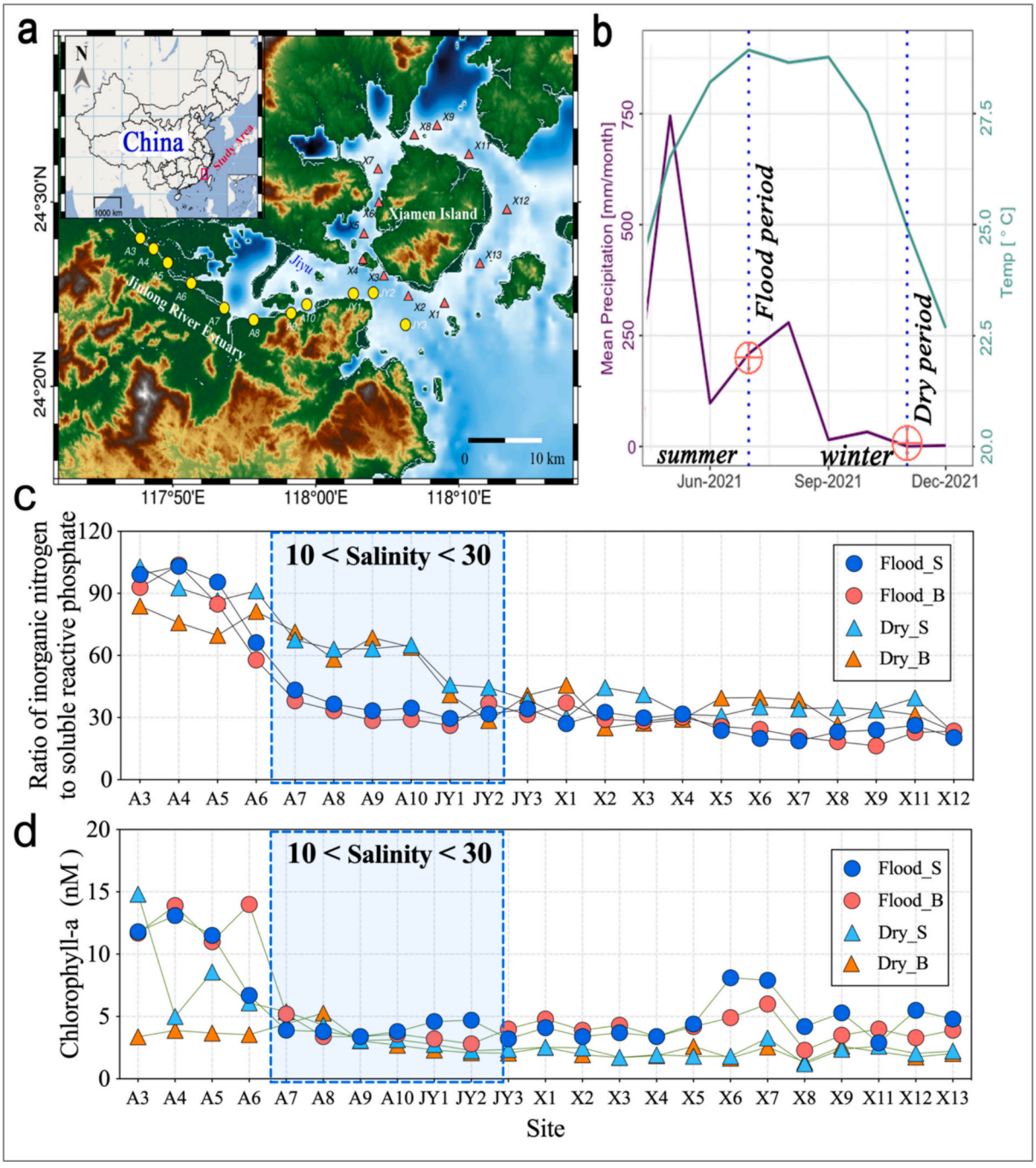

Fig. 1. Sampling locations and their basic characteristics in subtropical southeastern China in this study. (a) Study area and sampling sites at the surface and bottom waterbodies of Jiulong River Estuary (yellow dots) and the coastal area around Xiamen Island (red triangles), (b) Average monthly temperature and precipitation changes throughout June 2021 to December 2021. The left axis represents the mean precipitation level, whereas the right axis represents the mean temperature. The flood and dry periods samples were selected in July and November and labeled with blue dotted lines and red-cross dots. (c) and (d) The ratio of total inorganic nitrogen to soluble reactive phosphate (TIN/SRP) and the concentration of chlorophyll-a (Chl-a) across sampling sites, respectively. Flood_S = Flood period Surface, Flood_B = Flood period Bottom, Dry_S = Dry period Surface, and Dry_B = Dry period Bottom. The blue shadowed box represents a salinity (Sal) range from 10 to 30 PSU. The line connecting the points is provided to assist in visual interpretation. Data source: https://4dvd.sdsu.edu. (For interpretation of the references to color in this figure legend, the reader is referred to the web version of this article.)

microbial pterin concentrations and frozen at −20 °C before analysis. All water samples for dissolved nutrients were filtered through Whatman GF/F (0.7 mm, Cytiva, USA) glass microfiber filters on board and determined within 48 h in the lab.

2.3. Water physicochemical parameter analysis

Dissolved oxygen (DO) concentration and temperature, pH, and salinity were measured directly using a WTW multiparameter meter (Multi 3430, Germany) on board. Turbidity was determined directly using a portable turbidity meter (YSI®6600, USA) on site. The concentration of nutrients for soluble reactive phosphate (PO_4^{3-}), nitrate (NO_3^-),

and nitrite (NO_2^-) was determined by spectrophotometry using the AA3 automatic analyzer (AA3, Seal, Germany). Subsamples were added with 1 ‰ chloroform stored at 4 °C and measured concentration of NH_4^+ with indophenol blue spectrophotometry (Tri-223, Spectrum, China) at 25 °C (Huang et al., 2021). The concentration of total inorganic nitrogen (TIN) was calculated as the sum of NO_3^-, NO_2^-, and NH_4^+. Chemical oxygen demand (COD) was determined using potassium permanganate (KMnO4) as an oxidizing agent to oxidize organic matter in seawater samples at high temperatures following the same method described by (Wang and Wang, 2022).

2.4. Biological characteristics in suspended particles

2.4.1. Chlorophyll -a measure

The chl-a samples were filtered (~150 mL) directly with GF/F filters (Whatman) using a low-pressure pump (<150 mmHg). The chl-a samples were instantly immersed in liquid nitrogen and then stored at −80 °C before analysis. In the lab, the chl-a concentration was extracted by adding 5 mL of 90 % acetone (v/v) into filters and detected using a fluorescence detector (Turner Designs Fluorometer, USA) following the protocol described by the previous study (Liu et al., 2017).

2.4.2. Extraction of microbial pterins

We extracted microbial pterins in particulate samples following a method described in previous literature (Suffridge et al., 2017). All samples were mixed with 4 mL of cold lysis solution (5 % methanol in MQ, pH = 3.5) and 2 mL of zirconia/silica beads (5 mm, BioSpec, USA) in aseptic 15 mL polypropylene tubes. Cells were lysed by vortexing for 5 min followed by 1 min in an ice bath, repeated six times over 30 min. Pterins were extracted by ultrasonic bathing for 30 min in the dark at 30 °C. The sample pH was first adjusted to 6.5 using 0.1 M NaOH, and then added 4 mL pure chloroform (1:1, v/v), and finally vortexed for 3 min for hydrophilic pterins extraction. After centrifuging the sample for 10 min at 5000 rpm, the aqueous phase was transferred for a repeated chloroform extraction (Mashego et al., 2007). Samples were filtered using methanol-rinsed 0.2 μm filters, and were either analyzed within 48 h or stored at −20 °C.

2.4.3. Pterin determination

Chromatographic separation of neopterin (Nep), dihydro-neopterin (H2Nep), biopterin (Bip), and isoxanthopterin (Ixp) was conducted using a high-performance liquid chromatography (HPLC, Dionex Ultimate 3000, USA) system with a fluorescence detector (FLD), quaternary pump (LPG-3400 A), and Shimadzu VP-ODS column (4.6 × 250 mm, 5 μm). The mobile phase consisted of 10:90 (v/v) methanol: water, with a flow rate of 0.7 mL min^{-1} and a 20 μL injection volume. Fluorescence detection was performed at 350 nm excitation and 440 nm emission modified from the previous study (Koslinski et al., 2014). Pterin standards were obtained from Sigma-Aldrich Biotec. Ltd. (Darmstadt, Germany) and stored as instruction before assessment.

2.5. Indoor algae cultivation

Culture conditions for cyanobacteria *Synechococcus* WH7803 followed the referenced culture method (Guillard and Hargraves, 1993; Guillard and Morton, 2003). In brief, *Synechococcus* was cultured in L1 Medium (detailed in Table S1), diluted with filtered seawater from the South China Sea (SCS) at 20 ± 2 °C for 14 days. The light-dark illumination mode was 14 h:10 h (5000 lx). Four nutrient levels of N:P exposures (CK = 16:1, LL = 24:1, ML = 32:1, and HL = 64:1) were applied to the culture experiment to observe cyanobacteria responses. The culture conditions are detailed in Table S2. During the culture period, 10 mL algae samples were collected every two days, fixed with Lugol's iodine solution, and counted for cell abundance or stored at 4 °C (Zhang et al., 2023). For nutrient analysis, 30 mL samples were filtered through a 0.7 μm GF/F membrane and analyzed within 48 h or stored at −20 °C. Pterin samples (60 mL) were filtered with a PC membrane and stored at −80 °C for biopterin extraction and quantification as previously described. The polyethylene flasks, filtered seawater, and culture medium were sterilized using high-temperature, high-pressure steam to ensure experimental sterility. Cyanobacteria strains were supplied by the Center for Collections of Marine Bacteria Phytoplankton (CCMBP) at the State Key Laboratory of Marine Environmental Science, Xiamen University.

2.6. Statistical analysis

The significance of the measured parameters for each pterin was determined using one-way ANOVA. Differences in pterins were further analyzed with one-way ANOVA followed by Duncan's multiple comparison test. The Geisser-Greenhouse correction was applied to account for variance homogeneity. Significance was defined at the level of $p < 0.05$. Spearman's correlation analysis was used to identify relationships among parameters. Data statistics and visualizations were performed using the R statistics package (Version 4.0.2), SPSS Statistics 23.0, and GraphPad Prism 9. Genomic representative sequences for microbial composition analysis were classified based on operational taxonomic units using the meta micro-database on the cloud platform (https://magic.novogene.com/).

3. Results

3.1. Hydrological conditions and water chemistry changes

Monthly precipitation and temperature data for the JRE and XMB during the sampling period are shown in Fig. 1b. Total precipitation was approximately 1481.4 mm, with over 90 % occurring during the flood period (cruise in July 2021). The highest precipitation (~750 mm) was recorded in May, while the dry period (cruise in November 2021) had minimal rainfall (~2 mm). Bottom water temperatures in JRE and XMB during the flood period (29.3–33.9 °C) were significantly higher than in the dry period (20.5–22.5 °C). DO levels generally increased with salinity, with surface water showing higher DO than the bottom layer in both sampling cruises (Fig. S1c). COD was higher (2–6 mg L^{-1}) in the upper estuary with elevated organic matter occurrence, but decreased (<2 mg L^{-1}) with increasing salinity in the lower estuary and the XMB (Fig. S1e and f). The inorganic nitrogen (TIN) and soluble reactive phosphate (SRP) concentrations in the estuarine waters varied with salinity ranges during two cruises (Fig. S2). The upper estuary with low salinity (<10 PSU) was characterized with the highest N/P nutrients (TIN = 190.7–230 μM, SRP = 2.35–2.47 μM), compared to the middle (10–30 PSU, TIN = 43.2–105.2 μM, SRP = 1.29–1.76 μM) and high salinity sites (>30 PSU, TIN = 17.2–35.7 μM, SRP = 0.70–1.03 μM). Both nutrients exhibited similar trends in the surface and bottom waters in each cruise.

3.2. Distribution pattern of microbial pterins against salinity

The estuary is influenced by both freshwater runoff and tidal intrusion, with bottom-layer salinity in the JRE ranging from 2 to 33 PSU. Surface salinity in the XMB ranged from 29.2 to 33.5 PSU, while bottom salinity ranged from 29.9 to 32.8 PSU (Fig. S1a, b). The spatial distribution of Bip concentration showed a similar trend in both surface and bottom waters, decreasing against salinity outward from the estuary to the coastal region. Geographically, concentrations were higher in the JRE than in the XMB. Seasonally, Nep (Flood period: 6.6–31.2 pM; Dry period: 1.7–8.1 pM), H2Nep (Flood period: 0.86–64.4 pM; Dry period: 0.92–8.8 pM), and Ixp (Flood period: 2.4–136 pM; Dry period: 2.2–9.6 pM) were higher during the flood period than that of the dry period. In contrast, Bip showed no significant difference among each group, decreasing in the estuarine region but peaking with high salinity during the dry period in the XMB (Fig. 2c). There were no significant differences

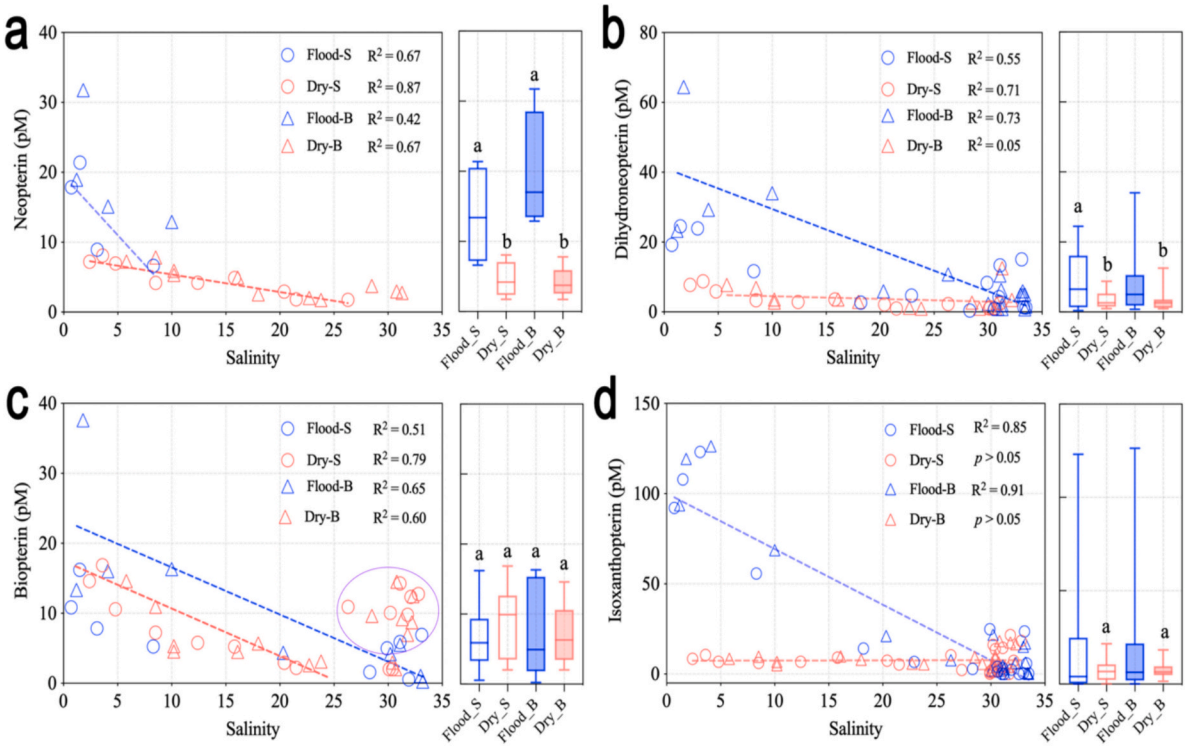

Fig. 2. Microbial pterin concentration changes along with salinity in the surface and the bottom waters of the Jiulong River Estuary and Coastal Xiamen Island. (a) Neopterin, (b) dihydro-neopterin, (c) biopterin, (d) isoxanthopterin. Flood_S = Flood period Surface, Flood_B = Flood period Bottom, Dry_S = Dry period Surface, and Dry_B = Dry period Bottom. Linear regression results between the pterin concentrations and salinity, indicated by R^2, were shown in the upper left corner, respectively. The blue and red dashed lines represent the linear regression result for the flood and dry seasons. Box plots on the right side of each figure indicate the distribution of microbial pterin concentrations for different periods and sampling positions. Different letters on the top of each box represent significant differences at the significance of $p < 0.05$. The purple circle represents the culling data before linear fitting. (For interpretation of the references to color in this figure legend, the reader is referred to the web version of this article.)

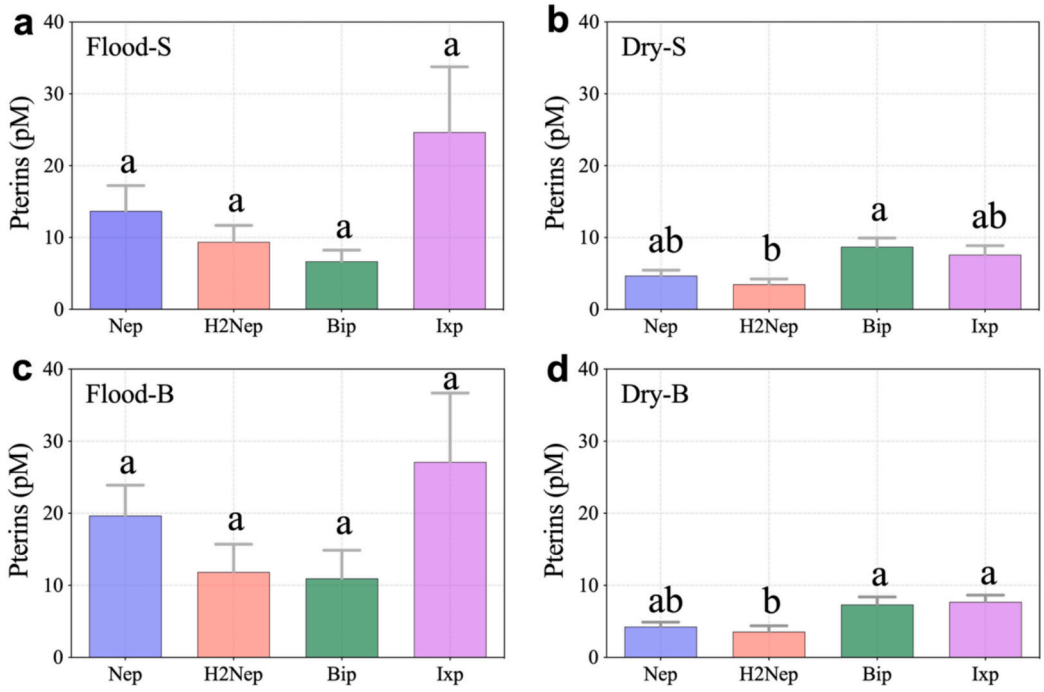

Fig. 3. Average concentration of four microbial pterins in the surface and bottom waters during different periods and sampling positions in this study. (a) Flood_S = Flood period Surface, (b) Flood_B = Flood period, (c) Bottom, Dry_S = Dry period Surface, and (d) Dry_B = Dry period Bottom. The purple, orange, green, and pink bars represent pterins neopterin (Nep), dihydro-neopterin (H2Nep), biopterin (Bip), and isoxanthopterin (Ixp), respectively. The error bars represent one standard deviation for all site samples (n = 23). Different letters on the top of each bar represent significant differences at the significance of $p < 0.05$. (For interpretation of the references to color in this figure legend, the reader is referred to the web version of this article.)

among pterin concentrations in both the surface and the bottom layers during the flood period. In contrast, significant differences were observed between H2Nep and Bip concentrations during the dry period (Table S2). Except for surface biopterin in the flood period, other pterins followed the trend: flood period > dry period. The pterin concentration during the flood period followed the order of Ixp > Nep > H2Nep > Bip, while in the dry period, pterin concentrations decreased and followed the order of Bip ≈ Ixp > Nep > H2Nep. In the surface layer, Bip was significantly higher than H2Nep ($p < 0.01$), and in the bottom layer, both Bip and Ixp were significantly higher than H2Nep ($p < 0.01$) (Fig. 3).

3.3. Distribution of chl-a and microbial composition

3.3.1. Variations of chl-a along with microbial pterins

The concentrations of chl-a were higher in the upper estuarine (A3-A7) of the JRE compared to the middle sites (A7-JY3) in the flood period. In the dry period, surface chl-a in the upper JRE was significantly higher than in the bottom layer. Overall, XMB exhibited higher chl-a concentrations during the flood period than during the dry period. The bottom chl-a near the estuarine mouth (X1-X4) was slightly elevated during the flood period, but no significant difference was found between the surface and bottom waters in the dry period (Fig. 1d).

In the flood period, no significant difference in chl-a concentrations

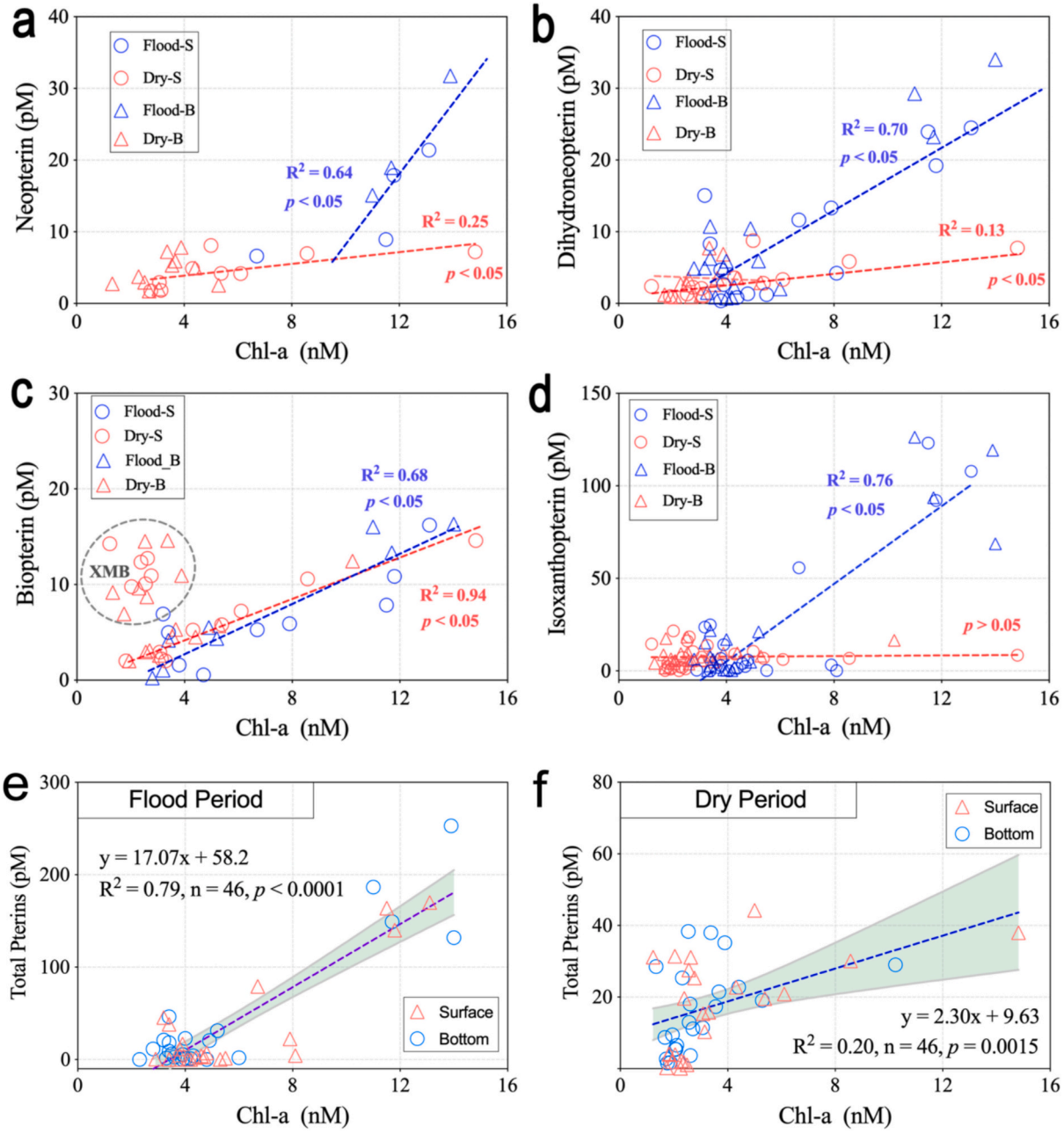

Fig. 4. Linear correlation of microbial pterins and chlorophyll-a (Chl-a) in the surface and the bottom waters of the Jiulong River Estuary and Coastal Xiamen Bay. (a) Neopterin vs Chl-a, (b) dihydro-neopterin vs Chl-a, (c) biopterin vs Chl-a, and (d) isoxanthopterin vs Chl-a. The blue and red dashed lines represent the linear regression result for the flood and dry seasons. The gray dashed circle in (c) represents the culling data before linear fitting. (e) and (f) show the relationship between total pterins and Chl-a in the flood period and dry period, respectively. The dark blue dashed lines represent the linear regression results with a 95 % confidential interval. The regression functions, along with statistical analysis, are displayed near the lines. (For interpretation of the references to color in this figure legend, the reader is referred to the web version of this article.)

was found between the surface and the bottom layers in the JRE. Higher surface chl-a in the sites of the XMB (X6-X13) were recorded than that in the bottom layers (Fig. 1d). A positive relationship was observed between Chl-a and Bip during the flood period for both surface and bottom layers (R^2 = 0.64–0.76, $p < 0.01$, Fig. 4a–d). Notably, Bip exhibited elevated concentrations even at low chl-a levels in the XMB (Fig. 4c, dashed gray circle). Total pterins positively correlated with chl-a in both the JRE ($R^2 = 0.79, p < 0.01$, Fig. 4e) and the XMB ($R^2 = 0.20, p < 0.01$, Fig. 4f).

3.3.2. In-situ microbial composition

Microbial genera for composition analysis in suspended particles from the JRE are shown in Fig. S3. Estuarine samples had higher OTU counts than outer bay samples (bottom > surface), sharing 39,663 OTUs, representing 9.83 % of the total 403,298 OTUs (Fig. S3a). The dominant genera were gammaproteobacteria, alphaproteobacteria, and betaproteobacteria, comprising 35–59 % of the microbial composition (Fig. S3b). The key genera in JRE suspended particles included *Synechococcus_sp._HK05* and *uncultured_Caudovirales_Phage* (Fig. S3c).

3.4. Pterin levels in microalgae in response to nutrient enrichment

Cell biomass concentration and cellular Bip content of cyanobacterial *Synechococcus* persistently increased over the culture period (Fig. 6a, b), with Bip content continuing to accumulate during the stationary phase (day 10 to day 14). The Bip concentration per cell initially ascended and then declined during the exponential phase, before increasing again in the stationary phase (Fig. 6c, d). *Synechococcus* in all treatments reached the end of the exponential growth phase by day 8, with nitrate addition significantly enhancing microalgal growth (Fig. 6a, e). Algal abundance in the high N/P treatments (32:1 and 64:1) was significantly higher ($p < 0.05$) compared to the low N/P treatment (16:1). Both SRP and nitrate were gradually depleted, with SRP dropping below the detection limit by day 14 (Fig. S5a, b). The N/P ratios across all treatments followed the order: 64:1 > 32:1 > 24:1 > 16:1 during the whole period (Fig. S5c).

4. Discussion

4.1. Responses of microbial pterins to geochemical variations

The average of pterin concentrations in the flood period followed the order of Ixp (2.4–136 pM) > Nep (6.6–31.2 pM) > H2Nep (0.86–64.4 pM) > Bip (0.23–37.6 pM), while in the dry period, Bip (2.01–16.9 pM), Ixp (2.2–9.6 pM) > Nep (1.7–8.1 pM), and H2Nep (0.92–8.8 pM). Significantly higher concentrations of microbial pterins in the flood period compared to the dry period demonstrated the rapid production of algal proliferation products due to the discharge of high nutrients (Figs. 1 and S2). The concentration of microbial pterins was higher in estuaries due to terrestrial nutrient inputs that support higher microbial biomass. The overall algal blooms in the estuary tend to increase due to nutrient enrichment from agricultural fertilizers and aquaculture, with changes varying by nutrient sources (Tanaka et al., 2021).

The level of Nep was below the detection limit in most high-salinity regions, this is likely because Nep was consumed to support microbial growth. Besides that, Nep could be partially reduced to H2Nep and serve as a synthetic precursor for Bip. Nep and Bip are synthesized from GTP as the substrate, with Nep acting as an intermediate or precursor for Bip in the enzymatic synthesis (Feirer and Fuqua, 2017; Huber et al., 1984). The Bip concentration decreased with salinity generally, but it showed high values in the XMB, suggesting that extra sources of pterins were likely caused by the red tide outbreaks (Chen et al., 2021). Pterins might exist as the reactive reduced forms (e. g. H_2Bip and H_4Bip) or their derivatives (pterin glucosides) in the intact algal cells (Forrest et al., 1958; Hatfield et al., 1961). A past work demonstrated that substantial levels of aromatic pterins (e.g., biopterin glucosides) are present in natural water samples or algal cells (Yanting Zuo et al., 2021). The two fused aromatic heterocyclic rings characterized the oxidized (aromatic) forms of pterins, enabling these biomolecules to emit blue “humic-like” fluorescence (Yanting Zuo et al., 2021).

During the flood period, Ixp concentrations negatively correlated (R^2 = 0.85–0.91) with the salinity from the estuary to the coastal sea, suggesting that freshwater runoff likely leads to the gradient distribution of microbial pterins. In contrast, during the dry period, Ixp concentrations (1.52–21.6 pM) were relatively stable across both surface and bottom layers. This could be revealed by lower concentrations of chl-a (< 4 nM, Fig. 4d), indicating low-level algal biomass associated with low Ixp production. Ixp, as a final metabolite in the pterin synthesis pathway (Hubby and Throckmorton, 1960; Taira and Nawa, 1958), not only accumulated as photopigments enhancing light sensitivity (Shavit et al., 2023) but served as sources of carbon and nitrogen, supporting microbial metabolism and growth (McNutt Jr, 1963).

4.2. Pterins as biomarkers to algal bloom coupled with chl-a

The average chl-a concentrations in both surface and bottom layers were 5.55 ± 3.23 nM during the flood period, which is 1.73 times higher than the dry period (3.21 ± 2.31 nM). Moreover, a high positive correlation between microbial pterins and Chl-a (R^2 = 0.79, $p < 0.01$, Fig. 4e) was observed during the flood period, indicating that photoautotrophic microbes (0.22–10 μm) could be the main contributors to microbial pterins, particularly in the summer. Cyanobacteria and blue-green alga were identified as sources of various cellular pterins and their derivatives (Forrest et al., 1958; Lee et al., 1999; Noguchi et al., 1999; Stravs et al., 2017; Wachi et al., 1995; Yanting Zuo et al., 2021). Pterin compounds like Bip glucoside were identified to protect the components of photosynthetic vesicles (chlorophyll *a*, phycocyanin, and carotenoids) in cyanobacteria from UV damage act as absorbing chromophore (Moon et al., 2010a, 2012; Saito et al., 2003). A recent study reported that high levels of Bip ranged from 0.85 nM to 11.8 nM caused by cyanobacterial blooms in natural lakes (Yanting Zuo et al., 2021). However, pterins are also known to be both biolabile and photodegradable (Serrano et al., 2012). Under UV-A irradiation, tetrahydrobiopterin in aqueous solution undergoes photooxidation, producing derivatives of 6-formylpterin, dihydropterin, or 6-carboxypterin as fluorescent photosensitizers (Lorente and Thomas, 2006; Serrano et al., 2012; Telegina et al., 2018; Vignoni et al., 2010). The dual nature of pterins—as both antioxidants and photosensitizers—underscores their complex roles in biological and photochemical systems (Dantola et al., 2017).

During the dry period, the average concentration of chl-a significantly declined, except for elevated levels of sites in the upper reaches (salinity <10), where Bip corresponded with chl-a in the JRE (Fig. 4c, f). In contrast, Bip concentrations were higher despite lower chl-a levels in the high-salinity sites of XMB (Fig. 4c, dashed circle), indicating that heterotrophic bacteria might serve as additional pterin sources during the dry season. These variations in pterin levels may not always reflect the actual rate of microbial production and utilization, as dynamic microbial activity can obscure the fluxes involved. Thus, more work is needed to continue on the elucidation of sources and biological significance of microbial pterins.

4.3. Influences of in-situ nutrients and environmental factors on offshore pterins

PCA revealed that the first two principal components (PC1 + PC2) explained 95.4 % of the total variance during the flood period, with samplings in both JRE and XMB clustering on the positive PC1 axis (Fig. 5a). PC1, accounting for 69.5 % of the variation, with significant positive correlations between nutrients and COD ($p < 0.01$), identifying nutrients (TIN and SRP) and COD as key environmental factors. Overall, salinity, DO, and pH were all positively correlated with nutrients in both

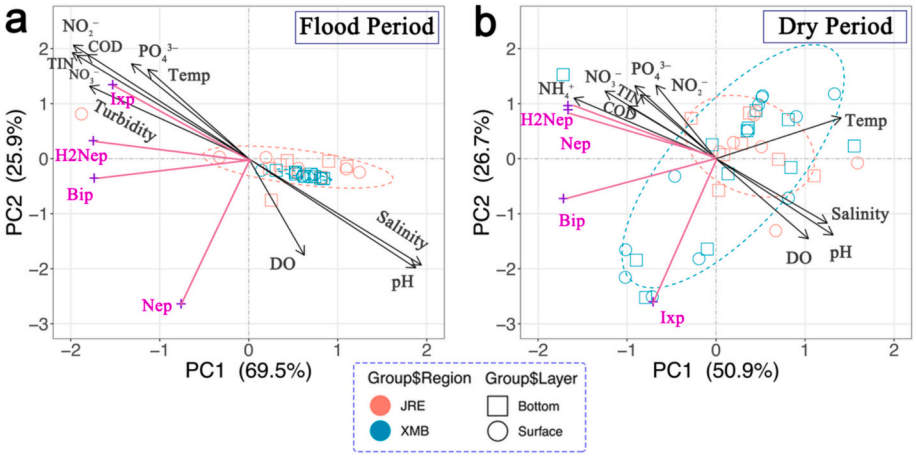

Fig. 5. Principal component analysis (PCA) results for determined parameters (a) and (b) in response to environmental factors of JRE-XMB during the flood period and the dry period, respectively. The pink loading lines represent the four microbial pterins, whereas the black arrows represent other environmental factors. SRP = Soluble Reactive Phosphate, TIN = Total Inorganic Nitrogen, TN = Total Nitrogen, TP = Total Phosphorus, and TPtn = Total Pterins.

flood and dry periods. During the flood period, microbial pterins (Bip, H2Nep, and Ixp) showed strong positive correlations with environmental factors (Temp, COD, and nutrients), whereas, in the dry period, Nep and H2Nep were significantly correlated with nutrients (Fig. 5b). PCA identified PC1 as being positively correlated with salinity and pH, and negatively correlated with Bip, H2Nep, and Ixp. PC2, which explained 25.9 % of the variance, showed positive correlations with nutrients, temperature, and COD. All samples (JRE + XMB) were centrally distributed along the positive axis and had higher positive PC1 scores (longer arrows), suggesting that freshwater runoff (PC1), as regulated by river flow, may be the key driver of biogeochemical processes and environmental conditions during the summer. Previous studies indicate that during the summer high runoff period in the Yangtze River Estuary, freshwater flow-driven estuarine mixing and nutrient inputs are crucial in regulating particulate organic matter (POM) dynamics in the nearshore surface regions (Qu et al., 2019, 2021).

During the dry period, the first two principal components (PC1 + PC2) explained 77.6 % of the variance. The JRE samples clustered along the positive PC1 axis, indicating a strong influence on terrestrial river inputs as well. In contrast, The XMB samples were dispersed across both positive and negative axes (Fig. 5b), suggesting the presence of additional biogeochemical factors, such as mixing processes and biological involvements (Chen et al., 2021), as regulatory influences. PC1 (50.9 % of variance) was positively correlated with temperature, salinity, pH, and DO, while PC2 (25.9 %) correlated with nutrient variations, indicating that the regulating factors were partially similar to those during the flood period. In general, Bip, H2Nep, and Ixp showed positive correlations with N/P nutrients, and positive couplings were observed between chl-a and microbial pterins (Fig. S4a, b). This suggests that nutrient inputs and freshwater-derived POM in the JRE, combined with high productivity, are key drivers of pterin dynamics.

4.4. Responses of microalgae and cellular pterin to nutrient stresses

Based on observational and experimental results, we designed cultivation experiments to investigate the dynamic responses of pterin concentrations to nutrient stress and to better understand algal growth status. Our results found that the biomass during the stationary phase of other high-nutrient experimental groups was 47.8–84 % higher than that of the control group. Higher N/P ratios were linked to greater algal abundance at the plateau (Fig. 6e), indicating that nutrient enrichment enhances carbon fixation by cyanobacteria. Despite this, Bip concentration remained roughly similar across all nutrient treatments except at N: P = 32: 1 (Fig. 6f), leading to microbial pterin consumption and (or) accumulation within the cells. In a recent study, the concentration of aqueous Bip rapidly declined in the presence of *Microcystis aeruginosa* under light/dark cycle irradiation, likely due to uptake by the microalgae (Yanting Zuo et al., 2021). In our study, Bip per cell first peaked on day 4 during the exponential growth phase across all treatments (Fig. 6d), indicating a preparatory stage for algal proliferation by utilizing pterin molecules. Pterins are ubiquitous biomolecules synthesized by bacteria and cyanobacteria and participate in various biological functions, acting as pigments and serving as essential cofactors in enzymatic redox reactions (Feirer and Fuqua, 2017). Furthermore, cellular Bip continued to increase even as *Synechococcus* biomass reached the plateau phase from day 10 to day 14 (Fig. 6c), suggesting a key role in biosynthetic processes that promote algal proliferation. The reduced forms 7,8-dihydrobiopterin (H_2Bip), and 5,6,7,8-tetrahydrobiopterin (H_4Bip) are crucial pterins in algal cells related to autoxidation and photooxidation, with Bip likely present as H_2Bip and H_4Bip (Buglak et al., 2021; Feirer and Fuqua, 2017; Saito et al., 2003; Wachi et al., 1995). H_4Bip acts as a natural cofactor essential for the hydroxylation of aromatic amino acids (phenylalanine, tyrosine, and tryptophan) (Feirer and Fuqua, 2017). While MoCo functions in some dissimilatory nitrate reductases involved in nitric oxide production, there is no direct evidence for H_4Bip's role in this process. Both H_2Bip and H_4Bip can oxidize to Bip when microbial pterins are extracted and exposed to atmospheric oxygen.

5. Conclusion

The temporal-spatial distribution of microbial pterins in estuarine and nearshore waters underscores their potential as biologically significant biomarkers. Elevated concentrations of microbial pterins at the upper estuary during the flood period, compared to the dry period, highlight their rapid production in response to nutrient-rich discharges that promote algal proliferation. Strong positive correlations between microbial pterins and chl-a suggest that photoautotrophic microbes (0.22–10 μm) are likely the primary contributors to microbial pterins, particularly in summer. Principal component analysis (PCA) indicates that freshwater runoff, regulated by river flow, is a key driver of biogeochemical processes and environmental conditions during the summer. Positive correlations of Bip, H2Nep, and Ixp with N/P nutrients, and the coupling between Chl-a and microbial pterins, reveal that higher N/P ratios enhance algal abundance and cyanobacterial carbon fixation, as well as cellular pterin synthesis. Cellular biopterin levels have peaked during the exponential growth phase of cyanobacterial

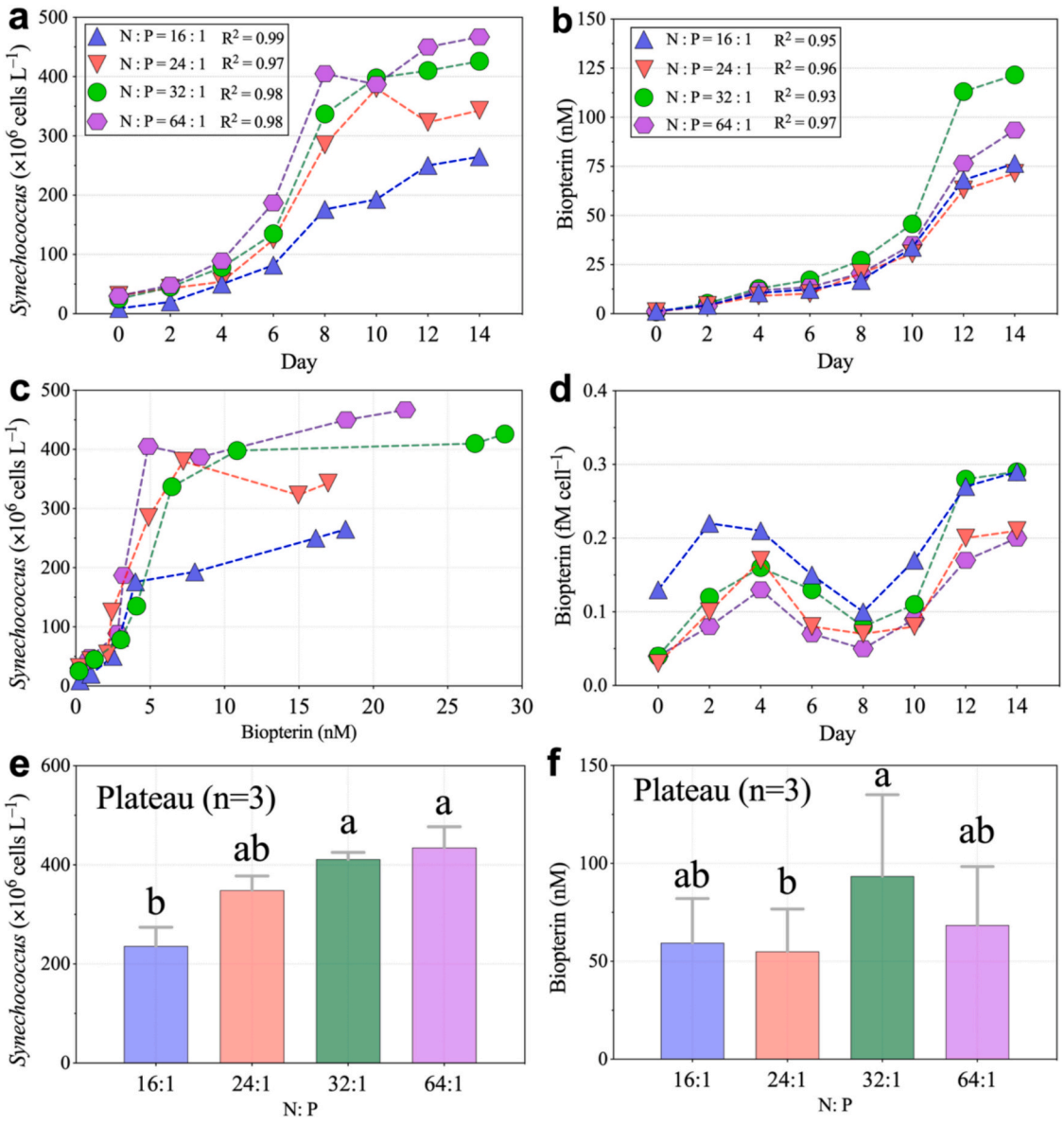

Fig. 6. Time-dependent variations at different nutrient levels of N:P exposure in the culture experiment. (a) Algae abundance of *Synechococcus*, (b) biopterin concentration, (c) plot of *Synechococcus* cell abundance and biopterin, (d) biopterin concentration per cell, (e) and (f) *Synechococcus* and biopterin abundance during the stationary phase of day 10 to day 14 as the plateau at different N:P (n = 3), respectively. Different letters on the top of each bar represent significant differences at the significance of $p < 0.05$.

cultivation. This accumulation may contribute to cellular metabolism and stress adaptation, potentially facilitating subsequent algal proliferation. It is worth mentioning that the dynamic equilibrium between the generation and consumption of microbial pterins reflects intracellular accumulation instantly rather than actual flux. As a dual biomarker with chl-a, microbial pterins can improve bloom detection specificity and provide insights into bloom dynamics and nutrient conditions. However, further research is necessary to clarify their implications and limitations as ecological indicators.

CRediT authorship contribution statement

Kang Mei: Writing – review & editing, Writing – original draft, Software, Methodology, Investigation, Funding acquisition, Formal analysis, Data curation, Conceptualization. **Yitong Pan:** Writing – review & editing, Writing – original draft, Visualization, Methodology. **Faisal Hamzah:** Writing – review & editing, Writing – original draft. **Mohammad Mazbah Uddin:** Writing – review & editing, Writing – original draft. **Xuri Dong:** Writing – review & editing, Writing – original draft. **Lizhe Cai:** Supervision, Resources, Project administration, Funding acquisition. **Bin Xie:** Methodology. **Nengwang Chen:** Supervision, Resources, Project administration, Funding acquisition. **Deli Wang:** Supervision, Resources, Project administration, Funding acquisition.

Declaration of Generative AI and AI-assisted technologies in the writing process

During the preparation of this work, the author(s) used ChatGpt (OpenAI) to improve the manuscript's linguistic expression and readability. After using this tool/service, the author(s) reviewed and edited the content as needed and take(s) full responsibility for the content of the publication.

Declaration of competing interest

The authors declare that they have no known competing financial

interests or personal relationships that could have appeared to influence the work reported in this paper.

Acknowledgment

This study was supported by the Jiangsu Natural Science Foundation (BK20241063), Natural Science Foundation of Xiamen (3502Z20227088) and the National Natural Science Foundation of China (NSFC) (grants 41476060 and U1805242). We extend our gratitude to Mengqiu Shi, Liuqian Qi, Haowen Zhong, and Wenmei Liu from Xiamen University for their assistance with sampling and laboratory processing. We thank the crew of Research Vessel Haiyang II for their sampling assistance. Special thanks to Professor Sergio A. Sañudo-Wilhelmy from the University of Southern California, USA, for his guidance and encouragement, inspiring me to continue research on pterins in marine science.

Appendix A. Supplementary data

Supplementary data to this article can be found online at https://doi.org/10.1016/j.marpolbul.2025.118137.

Data availability

Data will be made available on request.

References

Basu, P., Burgmayer, S.J., 2011. Pterin chemistry and its relationship to the molybdenum cofactor. Coord. Chem. Rev. 255, 1016–1038.
Batchelli, S., Muller, F.L., Chang, K.C., Lee, C.L., 2010. Evidence for strong but dynamic iron-humic colloidal associations in humic-rich coastal waters. Environ. Sci. Technol. 44, 8485–8490.
Buglak, A.A., Telegina, T.A., Vechtomova, Y.L., Kritsky, M.S., 2021. Autoxidation and photooxidation of tetrahydrobiopterin: a theoretical study. Free Radic. Res. 55, 499–509.
Bruland, K.W., Lohan, M.C., 2006. Controls of trace metals in seawate. Treatise on Geochemistry 6, 23–47.
Buglak, A.A., Kapitonova, M.A., Vechtomova, Y.L., Telegina, T.A., 2022. Insights into molecular structure of pterins suitable for biomedical applications. Int. J. Mol. Sci. 23, 15222.
Cai, W.-J., Feely, R.A., Testa, J.M., Li, M., Evans, W., Alin, S.R., Xu, Y.-Y., Pelletier, G., Ahmed, A., Greeley, D.J., 2021. Natural and anthropogenic drivers of acidification in large estuaries. Annu. Rev. Mar. Sci. 13, 23–55.
Chen, B.H., Kang, W., Xu, D., Hui, L., 2021. Long-term changes in red tide outbreaks in Xiamen Bay in China from 1986 to 2017. Estuar. Coast. Shelf Sci. 249.
Dantola, M.L., Reid, L.O., Castaño, C., Lorente, C., Oliveros, E., Thomas, A.H., 2017. Photosensitization of peptides and proteins by pterin derivatives. Pteridines 28, 105–114.
Enchev, V., Slavova, S., 2021. Self-catalytic mechanism of prebiotic reactions: from formamide to pterins and guanine. Phys. Chem. Chem. Phys. 23, 19043–19053.
Fang, Z., Wang, W.X., 2022. Dynamics of trace metals with different size species in the Pearl River Estuary, Southern China. Sci. Total Environ. 807, 150712.
Feirer, N., Fuqua, C., 2017. Pterin function in bacteria. Pteridines 28, 23–36.
Forrest, H.S., Van Baalen, C., Myers, J., 1958. Isolation and identification of a new pteridine from a blue-green alga. Arch. Biochem. Biophys. 78, 95–99.
Guillard, R., Hargraves, P., 1993. Stichochrysis immobilis is a diatom, not a chrysophyte. Phycologia 32, 234–236.
Guillard, R., Morton, S., 2003. Culture methods. In: Manual on Harmful Marine Microalgae. UNESCO, Paris, pp. 77–97.
Guo, W.D., 2005. Fluorescent characteristics of colored dissolved organic matter (CDOM) in the Jiulong River estuary. Oceanol. Limnol. Sin. 36, 349–357.
Han, Guilin, 2019. Source identification and water-quality assessment of dissolved heavy metals in the Jiulongjiang River, Southeast China. J. Coast. Res. 36 (2), 403. https://doi.org/10.2112/JCOASTRES-D-19-00068.1.
Hatfield, D., Van Baalen, C., Forrest, H., 1961. Pteridines in blue green algae. Plant Physiol. 36, 240.
Huang, R., Sun, J., Yang, Y., Jiang, X., Wang, Z., Song, X., Wang, T., Zhang, D., Li, H., Yi, X., 2021. Elevated pCO2 impedes succession of phytoplankton community from diatoms to dinoflagellates along with increased abundance of viruses and bacteria. Front. Mar. Sci. 8, 642208.
Hubby, J.L., Throckmorton, L.H., 1960. Evolution and pteridine metabolism in the genus Drosophila. Proc. Natl. Acad. Sci. 46, 65–78.
Huber, C., Batchelor, J.R., Fuchs, D., Hausen, A., Lang, A., Niederwieser, D., Reibnegger, G., Swetly, P., Troppmair, J., Wachter, H., 1984. Immune response-associated production of neopterin. Release from macrophages primarily under control of interferon-gamma. J. Exp. Med. 160, 310–316.
Jing, Z., 1995. Geochemistry of trace metals from Chinese river/estuary systems: an overview. Estuar. Coast. Shelf Sci. 41, 631–658.
Koslinski, P., Jarzemski, P., Markuszewski, M.J., Kaliszan, R., 2014. Determination of pterins in urine by HPLC with UV and fluorescent detection using different types of chromatographic stationary phases (HILIC, RP C8, RP C18). J. Pharm. Biomed. Anal. 91, 37–45.
Lee, H.W., Oh, C.H., Geyer, A., Pfleiderer, W., Park, Y.S., 1999. Characterization of a novel unconjugated pteridine glycoside, cyanopterin, in *Synechocystis* sp. PCC 6803. Biochimica et Biophysica Acta (BBA)-bioenergetics 1410, 61–70.
Liu, N., Tong, S., Yi, X., Li, Y., Li, Z., Miao, H., Wang, T., Li, F., Yan, D., Huang, R., Wu, Y., Hutchins, D.A., Beardall, J., Dai, M., Gao, K., 2017. Carbon assimilation and losses during an ocean acidification mesocosm experiment, with special reference to algal blooms. Mar. Environ. Res. 129, 229–235.
Lorente, C., Thomas, A.H., 2006. Photophysics and photochemistry of pterins in aqueous solution. Accounts of Chemical Research Journal 39, 395–402.
Lorente, C., Serrano, M.P., Vignoni, M., Dántola, M.L., Thomas, A.H., 2021. A model to understand type I oxidations of biomolecules photosensitized by pterins. Journal of Photochemistry and Photobiology 7, 100045.
Ma, S., Han, G., 2024. Distribution, provenance, contamination, and probabilistic ecological risk of rare earth elements in surface sediments of Jiulong River estuary and adjacent watershed. Ocean Coast. Manag. 254, 107205.
Mahendran, R., Bs, S., Thandeeswaran, M., kG, K., Vijayasarathy, M., Angayarkanni, J., Muthusamy, G., 2020. Microbial (enzymatic) degradation of cyanide to produce pterins as cofactors. Curr. Microbiol. 77 (4), 578–587. https://doi.org/10.1007/s00284-019-01694-9.
Mao, S.-H., Zhang, H.-H., Zhuang, G.-C., Li, X.-J., Liu, Q., Zhou, Z., Wang, W.-L., Li, C.-Y., Lu, K.-Y., Liu, X.-T., 2022. Aerobic oxidation of methane significantly reduces global diffusive methane emissions from shallow marine waters. Nat. Commun. 13, 7309.
Marín-Yaseli, M.R., Mompeán, C., Ruiz-Bermejo, M., 2015. A prebiotic synthesis of pterins. Chem. Eur. J. 21, 13531–13534.
Martin, W., Russell, M.J., 2007. On the origin of biochemistry at an alkaline hydrothermal vent. Philos. Trans. R. Soc. B 362, 1887–1926.
Mashego, M.R., Rumbold, K., Mey, M., Vandamme, E., Soetaert, W., Heijnen, J.J., 2007. Microbial metabolomics: past, present and future methodologies. Biotechnol. Lett. 29, 1–16.
Matsunaga, T., Burgess, J.G., Yamada, N., Komatsu, K., Yoshida, S., Wachi, Y., 1993. An ultraviolet (UV-A) absorbing biopterin glucoside from the marine planktonic Cyanobacterium oscillatoria sp. Appl. Microbiol. Biotechnol. 39, 250–253.
McNutt Jr., W.S., 1963. The metabolism of isoxanthopterin by Alcaligenes faecalis. J. Biol. Chem. 238, 1116–1121.
Mei, K., Shi, M., Chen, N., Wang, D., 2024. Dynamics and geochemical responses of dissolved metals (Mn and Cu) in a subtropical estuary, China. Environ. Sci. Pollut. Res. 31, 6082–6093.
Menor-Salván, C., Burcar, B.T., Bouza, M., Fialho, D.M., Fernández, F.M., Hud, N.V., 2022. A shared prebiotic formation of neopterins and guanine nucleosides from pyrimidine bases. Chem. Eur. J. 28, e202200714.
Moon, Y.-J., Kim, S.-J., Park, Y.M., Chung, Y.-H., 2010a. Sensing UV/blue: pterin as a UV-A absorbing chromophore of cryptochrome. Plant Signal. Behav. 5, 1127–1130.
Moon, Y.-J., Lee, E.-M., Park, Y.M., Park, Y.S., Chung, W.-I., Chung, Y.-H., 2010b. The role of cyanopterin in UV/blue light signal transduction of cyanobacterium Synechocystis sp. PCC 6803 phototaxis. Plant Cell Physiol. 51, 969–980.
Moon, Y.-J., Kim, S.I., Chung, Y.-H., 2012. Sensing and responding to UV-A in cyanobacteria. Int. J. Mol. Sci. 13, 16303–16332.
Noguchi, Y., Ishii, A., Matsushima, A., Haishi, D., Yasumuro, K., Moriguchi, T., Wada, T., Kodera, Y., Hiroto, M., Nishimura, H., Sekine, M., Inada, Y., 1999. Isolation of biopterin-alpha-glucoside from Spirulina (Arthrospira) platensis and its physiologic function. Mar. Biotechnol. 1, 207–210.
Oliveros, E., Dántola, M.L., Vignoni, M., Thomas, A.H., Lorente, C., 2010. Production and quenching of reactive oxygen species by pterin derivatives, an intriguing class of biomolecules. Pure Appl. Chem. 83, 801–811.
Pan, F., Cai, Y., Guo, Z., Fu, Y., Wu, X., Liu, H., Wang, X., 2021. Kinetic characteristics of mobile Mo associated with Mn, Fe and S redox geochemistry in estuarine sediments. J. Hazard. Mater. 418, 126200.
Petroselli, G., Dántola, M.L., Cabrerizo, F.M., Capparelli, A.L., Lorente, C., Oliveros, E., Thomas, A.H., 2008. Oxidation of 2′-deoxyguanosine 5′-monophosphate photoinduced by pterin: type I versus type II mechanism. J. Am. Chem. Soc. 130, 3001–3011.
Pokrovsky, O.S., Shirokova, L.S., Viers, J., Gordeev, V.V., Shevchenko, V.P., Chupakov, A.V., Vorobieva, T.Y., Candaudap, F., Causserand, C., Lanzanova, A., 2014. Fate of colloids during estuarine mixing in the Arctic. Ocean Sci. 10 (1), 107–125. https://doi.org/10.5194/os-10-107-2014.
Powell, Rodney T., Landing, William M., Bauer, James E., 1996. Colloidal trace metals, organic carbon and nitrogen in a southeastern U.S. estuary. Mar. Chem. 55 (1–2), 165–176.
Qu, D., Yu, H., Sun, Y., Zhao, Y., Wei, Q., Yu, H., Kelly, R.M., Yuan, Y., 2019. Numerical study on the summertime patches of red tide in the adjacent sea of the Changjiang (Yangtze) River Estuary, China. Mar. Pollut. Bull. 143, 242–255.
Qu, L., Jiao, T., Guo, W., Dahlgren, R.A., Ling, N., Feng, B., 2021. Hydro-biogeochemical alterations to optical properties of particulate organic matter in the Changjiang Estuary and adjacent shelf area. Ecol. Indic. 128, 107837.
Rodriguez, L.E., Weber, J.M., Barge, L.M., 2024. Evaluating pigments as a biosignature: abiotic/prebiotic synthesis of pigments and pigment mimics in planetary environments. Astrobiology 24, 767–782.
Roy, M., Martin, J.B., Smith, C.G., Cable, J.E., 2011. Reactive-transport modeling of iron diagenesis and associated organic carbon remineralization in a Florida (USA) subterranean estuary. Earth Planet. Sci. Lett. 304, 191–201.

Saito, T., Ishikura, H., Hada, Y., Fukui, K., Kodera, Y., Matsushim, A., Inada, Y., 2003. Photostabilization of phycocyanin and anthocyanin in the presence of biopterin-α-glucoside from Spirulina platensis under ultraviolet ray. Dyes Pigments 56, 203–207.

Salcedo, A.J.M., Prat, N., Bertrans-Tubau, L., Piñero-Fernandez, M., Cunillera-Montcusí, D., López-Doval, J.C., Abril, M., Proia, L., Cañedo-Argüelles, M., 2024. What happens when salinization meets eutrophication? A test using stream microcosms. Sci. Total Environ. 912, 168824.

Serrano, M.P., Lorente, C., Vieyra, F.E., Borsarelli, C.D., Thomas, A.H., 2012. Photosensitizing properties of biopterin and its photoproducts using 2′-deoxyguanosine 5′-monophosphate as an oxidizable target. Phys. Chem. Chem. Phys. 14, 11657–11665.

Serrano, M.P., Lorente, C., Borsarelli, C.D., Thomas, A.H., 2015. Unraveling the degradation mechanism of purine nucleotides photosensitized by pterins: the role of charge-transfer steps. ChemPhysChem 16, 2244–2252.

Serrano, M.P., Estébanez, S., Vignoni, M., Lorente, C., Vicendo, P., Oliveros, E., Thomas, A.H., 2017. Photosensitized oxidation of 2′-deoxyguanosine 5′-monophosphate: mechanism of the competitive reactions and product characterization. New J. Chem. 41, 7273–7282.

Shavit, K., Wagner, A., Schertel, L., Farstey, V., Akkaynak, D., Zhang, G., Upcher, A., Sagi, A., Yallapragada, V.J., Haataja, J., 2023. A tunable reflector enabling crustaceans to see but not be seen. Science 379, 695–700.

Stravs, M.A., Pomati, F., Hollender, J., 2017. Exploring micropollutant biotransformation in three freshwater phytoplankton species. Environ Sci Process Impacts 19, 822–832.

Suffridge, C., Cutter, L., Sanudo-Wilhelmy, S.A., 2017. A new analytical method for direct measurement of particulate and dissolved B-vitamins and their congeners in seawater. Front. Mar. Sci. 4, 11.

Taira, T., Nawa, S., 1958. No direct metabolic relation between pterines and uric acid, flavins or folic acid in Drosophila melanogaster. The Japanese Journal of Genetics 33, 42–45.

Tanaka, Y., Minggat, E., Roseli, W., 2021. The impact of tropical land-use change on downstream riverine and estuarine water properties and biogeochemical cycles: a review. Ecol. Process. 10, 40.

Telegina, T.A., Lyudnikova, T.A., Buglak, A.A., Vechtomova, Y.L., Biryukov, M.V., Demin, V.V., Kritsky, M.S., 2018. Transformation of 6-tetrahydrobiopterin in aqueous solutions under UV-irradiation. J. Photochem. Photobiol. A Chem. 354, 155–162.

Thomas, A.H., Lorente, C., Capparelli, A.L., Martínez, C.G., Braun, A.M., Oliveros, E., 2003. Singlet oxygen (1 Δ g) production by pterin derivatives in aqueous solutions. Photochem. Photobiol. Sci. 2, 245–250.

Uddin, M.M., Mei, K., Xie, B., Cunlu, L., Long, S., Xu, F., 2024. How does mangrove restoration or reforestation change trace metal pollution in mangrove ecosystems? A review of current knowledge. Toxics 12, 812.

Vignoni, M., Cabrerizo, F.M., Lorente, C., Claparols, C., Oliveros, E., Thomas, A.H., 2010. Photochemistry of dihydrobiopterin in aqueous solution. Org. Biomol. Chem. 8, 800–810.

Wachi, Y., Burgess, J.G., Iwamoto, K., Yamada, N., Nakamura, N., Matsunaga, T., 1995. Effect of ultraviolet-a (UV-a) light on growth, photosynthetic activity and production of biopterin glucoside by the marine UV-a resistant cyanobacterium *Oscillatoria* sp. BBA-Gen. Subj. 1244 (1), 165–168. https://doi.org/10.1016/0304-4165(94)00219-n.

Wang, W.H., Wang, W.X., 2016. Phase partitioning of trace metals in a contaminated estuary influenced by industrial effluent discharge. Environ. Pollut. 214, 35–44.

Wang, L.K., Wang, M.-H.S., 2022. COD determination and cleaning solution preparation using potassium permanganate for hazardous waste minimization. Evolutionary Progress in Science, Technology, Engineering, Arts, and Mathematics (STEAM) 1–41.

Wang, D., Aller, R.C., Wilhelmy, S., 2011. Redox speciation and early diagenetic behavior of dissolved molybdenum in sulfidic muds. Mar. Chem. 125, 101–107.

Wang, D.L., Lin, W.F., Yang, X.Q., Zhai, W.D., Dai, M.H., Chen, C.T.A., 2012. Occurrences of dissolved trace metals (Cu, Cd, and Mn) in the Pearl River Estuary (China), a large river-groundwater-estuary system. Cont. Shelf Res. 50-51, 54–63.

Wang, W.H., Chen, M., Guo, L.D., Wang, W.X., 2017. Size partitioning and mixing behavior of trace metals and dissolved organic matter in a South China estuary. Sci. Total Environ. 603, 434–444.

Yanting Zuo, A., Ji, W.A., Shi, C.A., Mhc, A., Yzh, A., Wxj, A., Yan, L.A., Zlh, B., Gk, C., Wtl, A., 2021. Identification of pterins as characteristic humic-like fluorophores released from cyanobacteria and their behavior and fate in natural and engineered water systems. Chem. Eng. J. 428.

Yu, D., Chen, N.W., Krom, M.D., Lin, J.J., Cheng, P., Yu, F.L., Guo, W.D., Hong, H.S., Gao, X.J., 2019. Understanding how estuarine hydrology controls ammonium and other inorganic nitrogen concentrations and fluxes through the subtropical Jiulong River Estuary, SE China under baseflow and flood-affected conditions. Biogeochemistry 142, 443–466.

Zhang, C., McIntosh, K.D., Sienkiewicz, N., Stelzer, E.A., Graham, J.L., Lu, J., 2023. Using cyanobacteria and other phytoplankton to assess trophic conditions: a qPCR-based, multi-year study in twelve large rivers across the United States. Water Res. 235, 119679.

Zhao, X., Cai, L., Rao, Y., Yang, D., Zhou, X., Wang, D., Mei, K., 2024. Comparison of macrozoobenthic communities and environmental variables in the subtidal zones between a nearly closed bay and an open bay. Reg. Stud. Mar. Sci. 73, 103464.